Joule heating characteristics of emulsion-templated graphene aerogels

Robert Menzel, Suelen Barg, Miriam Miranda, David B. Anthony, Salem M. Bawaked, Mohamed Mokhtar, Shaeel A. Al-Thabaiti, Sulaiman N. Basahel, Eduardo Saiz, Milo S. P. Shaffer

Joule Heating Characteristics of Emulsion-Templated Graphene Aerogels

Robert Menzel,* Suelen Barg, Miriam Miranda, David B. Anthony, Salem M. Bawaked, Mohamed Mokhtar, Shaeel A. Al-Thabaiti, Sulaiman N. Basahel, Eduardo Saiz, and Milo S. P. Shaffer*

The Joule heating properties of an ultralight nanocarbon aerogel are investigated with a view to potential applications as energy-efficient, local gas heater, and other systems. Thermally reduced graphene oxide (rGO) aerogels (10 mg cm⁻³) with defined shape are produced via emulsion-templating. Relevant material properties, including thermal conductivity, electrical conductivity and porosity, are assessed. Repeatable Joule heating up to 200 °C at comparatively low voltages (≈1 V) and electrical power inputs (≈2.5 W cm⁻³) is demonstrated. The steady-state core and surface temperatures are measured, analyzed and compared to analogous two-dimensional nanocarbon film heaters. The assessment of temperature uniformity suggests that heat losses are dominated by conductive and convective heat dissipation at the temperature range studied. The radial temperature gradient of an uninsulated, Joule-heated sample is analyzed to estimate the aerogel's thermal conductivity (around 0.4 W m⁻¹ K⁻¹). Fast initial Joule heating kinetics and cooling rates (up to 10 K s⁻¹) are exploited for rapid and repeatable temperature cycling, important for potential applications as local gas heaters, in catalysis, and for regenerable of solid adsorbents. These principles may be relevant to wide range of nanocarbon networks and applications.

1. Introduction

Nanocarbons, such as carbon nanotubes and graphene, are some of the most widely studied nanostructured materials due to their unique combination of electrical,[1] thermal[2] and mechanical[3] properties. Assembling low-dimensional nanocarbons into three-dimensional architectures creates new nanocarbon bulk materials that integrate the intriguing properties of the individual carbon nanostructures with the unique characteristics of porous networks, such as high surface-area- to-volume ratios, light weight and hierarchical microstructure. Nanocarbon aerogels have been produced via a range of approaches, but, most typically, through lyophilisation of wet-gel precursors formed from nanocarbon suspensions. These approaches have been used to produce ultralight bulk materials with wide variety of microstructures ranging from isotropic, nanoporous assemblies to ordered, macroscopic cellular networks.[4] These 3D nanocarbon bulk materials hold technological promise for a wide range of applications, including energy storage,[5] sensors,[6] catalyst supports,[7] and environmental applications, such as sorption, filtration, and separation technologies.[8]

A highly interesting feature of nanocarbon aerogels, in this context, is their potential to be directly heated through the application of electrical current (Joule heating). The study of nanocarbon Joule heating has mainly been focused on individual nanostructures, such as single-wall carbon nanotubes and graphene ribbons, often investigated in context of structural breakdown of the graphitic structure at high currents.[9] On a macroscopic scale, a range of reports have investigated direct resistive heating of two-dimensional nanocarbon films for applications as transparent, flexible film heaters.[10] However, the Joule heating of three-dimensional nanocarbon assemblies has been reported less frequently. In the context of polymer nanocomposites, direct electrical heating of 3D nanocarbon networks within an epoxy matrix has been used for polymer curing[11] and for the monitoring of structural damage and inhomogeneities via thermal IR imaging.[12] Direct resistive heating has also been utilized to thermally regenerate graphene aerogels used for gas sensing.[6a] However, the full potential of Joule heating of 3D nanocarbon assemblies has not yet been accessed due to a lack of understanding of the Joule heating properties of nanocarbon 3D assemblies. Specific applications for Joule-heated nanocarbon aerogels can be envisaged as direct, through-flow heaters in the field

Dr. R. Menzel, Dr. D. B. Anthony, Prof. M. S. P. Shaffer
Department of Chemistry
Imperial College London
London, SW7 2AZ, UK
E-mail: Robert.menzel04@imperial.ac.uk;
m.shaffer@imperial.ac.uk

Dr. R. Menzel
Bio Nano Consulting
The Gridiron Building
One Pancras Square, London, N1C 4AG, UK

Dr. S. Barg, Dr. M. Miranda, Prof. E. Saiz
Centre for Advanced Structural Ceramics
Department of Materials
Imperial College London
London, SW7 2AZ, UK

Ass. Prof. S. M. Bawaked, Prof. M. Mokhtar,
Prof. S. A. Al-Thabaiti, Prof. S. N. Basahel
Department of Chemistry
King Abdulaziz University
Jeddah 21589, Saudi Arabia
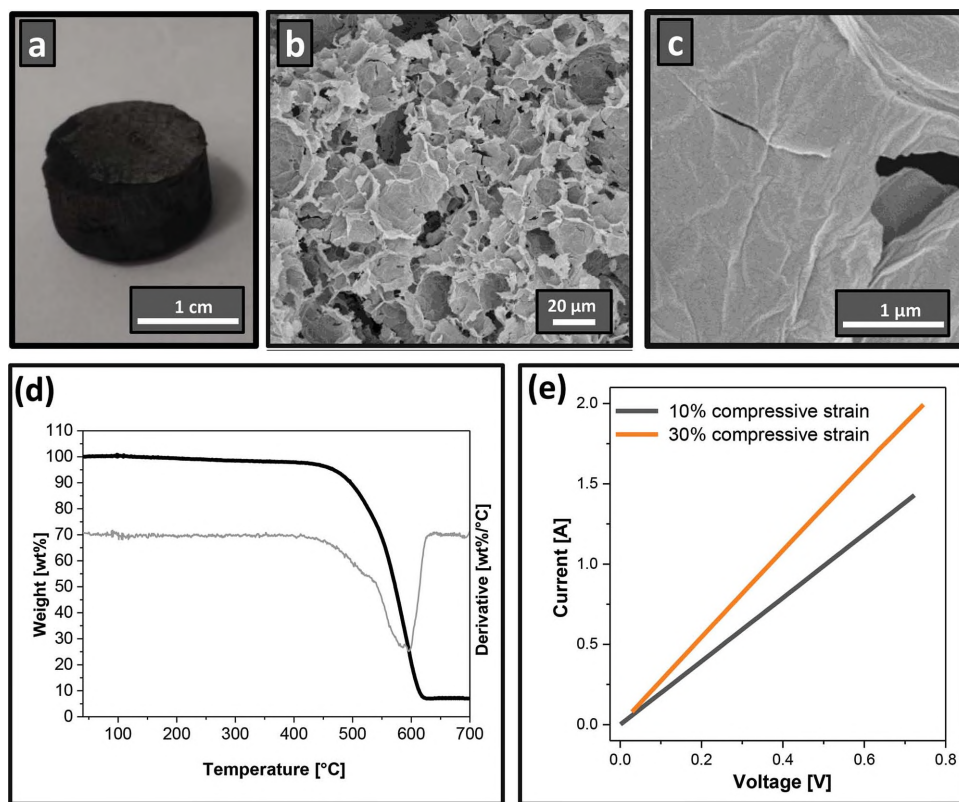
Figure 1. Morphological, thermal and electrical characterisation of rGO aerogel: a) photograph of cylindrical aerogel monolith; b,c) high and low-resolution scanning electron microscopy images of aerogel microstructure; d) thermal stability (thermogravimetric profile and derivative) in air; e) aerogel *I–V* curves at 25 mV s^{-1}, at two different compression strains.

of catalysis, sorption and sensing. The three-dimensional structure of the graphitic aerogel framework can enable uniform heating throughout the bulk material, thereby, reducing temperature gradients compared to classic external, radiative heating, resulting in a more energy-efficient and homogeneous heating process. The exceptional electrical and thermal properties of nanocarbons should enable fast heating and cooling kinetics, desirable for applications that require extensive temperature cycling.

This paper investigates the Joule heating characteristics of reduced graphene oxide (rGO) aerogels with densities of around 10 mg cm^{-3}, typical for ultralight three-dimensional nanocarbon assemblies. Bulk materials of defined shape are produced from highly concentrated GO-stabilised oil/water emulsions—a recently established methodology that allows the fabrication of mechanically robust aerogel monoliths with controlled shape, dimensions, and microstructure.[13] The morphological, electrical and thermal properties of the resulting aerogels, important characteristics for practical applications as flow-through gas heaters, are determined. The Joule-heating properties of the cylindrical, porous rGO aerogel monoliths are measured in a custom-made setup. Steady-state measurements of the surface and core temperature are performed to study reversibility and power-temperature characteristics. Further, Joule heating kinetics and temperature uniformity are investigated, discussed in terms of heat dissipation pathways and compared to the characteristics of two-dimensional nanocarbon

assemblies. Finally, rapid and repeatable temperature cycling of the rGO aerogel is demonstrated.

2. Results and Discussion

2.1. Morphological, Electrical, and Thermal Characterisation

Cylindrical aerogel monoliths with defined dimensions (**Figure 1**a) were produced via freeze-drying of concentrated GO Pickering emulsions in a mold, followed by high-temperature thermal reduction.[13]

Aerogel properties, relevant for potential applications as local Joule heaters, are given in **Table 1**. The rGO aerogel envelope density, as determined by the quotient of envelop volume and monolith mass, was 12 mg cm^{-3}, a typical value for low-density

Table 1. Structural, thermal and electrical characterisation data for the rGO aerogel.

	ρ_{env} [mg cm^{-3}][a]	ρ_{sk} [mg cm^{-3}][b]	σ [S m^{-1}][c]	c_p [J g^{-1} K^{-1}][d]	k [W m^{-1} K^{-1}][e]
rGO	12	930 ± 60	64 ± 2	1.73 ± 0.02	0.10 ± 0.01

[a]Aerogel envelop density; [b]aerogel framework density, determined via gas displacement; [c]electrical through-volume conductivity; [d]specific heat capacity, as determined by laser flash methodology; [e]thermal conductivity, as determined via laser flash methodology.

nanocarbon aerogels reported in the literature.[4a]-c The skeleton density of the aerogel, as measured by gas displacement, was determined to be 930 mg cm^{-3}. This value is considerably smaller than the density of graphite (around 2100 mg cm^{-3}). While GO can exhibit low bulk densities (around 1400 mg cm^{-3}),[14] the low skeletal density suggests a small amount of enclosed porosity, probably caused by wrinkling and irregular stacking of the graphene sheets upon assembly and thermal reduction. However, the accessible rGO aerogel porosity, as estimated from the difference in envelope and skeleton density, is very high at around 99% of the total monolith volume. SEM imaging (Figure 1b) of the aerogel microstructure (Figure 1b,c) was in good agreement with this finding. Low-resolution SEM showed the characteristic cellular microstructure of emulsion-templated aerogels, reflecting the assembly and densification of GO at the surface of the micrometer-sized emulsion droplets during aerogel fabrication. However, tears and pores (usually <1 μm) in the cell walls ensure full interconnectivity of the gas volume within the aerogel (in agreement with the high accessible porosity), an essential feature for applications such as gas adsorption and gas heating. Further, BET measurements indicate a moderately large, accessible specific surface area of around 200 m^2 g^{-1}, comparable to other thermally reduced graphene aerogels reported in the literature,[15,16] making this rGO aerogel an interesting candidate for applications in catalysis and adsorption. The electrical conductivity of the rGO monolith is high at 64 S m^{-1}, comparable to the best CNT and graphene aerogels produced in the literature,[17] an important requisite for efficient Joule heating at low input voltages. It is noteworthy that the electrical resistance decreases with monolith compression (as indicated by the increased gradient of the I-V curve in Figure 1e). Similar findings have been reported for other nanocarbon aerogels and are likely to be connected with increased contact area between the rGO sheets upon compression caused by buckling deformation of the aerogel cell walls.[17a] However, the effect of compression (within the reversible elastic regime) on to the Joule heating characteristics is relatively minor (Supporting Information, Figure S2, Table S1,S2). The specific heat capacity of the rGO aerogel is relatively high at 1.73 J g^{-1} K^{-1}, compared to high-quality graphite (0.7 J g^{-1} K^{-1}), due to significant imperfections in the graphitic lattice of thermally reduced graphene oxide. At 0.10 W m^{-1} K^{-1}, the thermal conductivity of the rGO aerogel is comparable to other porous nanocarbon 3D assemblies.[18] While low compared to the uniquely high values of individual nanocarbon structures, the thermal conductivity of the rGO aerogels is at least an order of magnitude higher compared to thermally insulating, non-graphitic aerogels, such as silica foams, which is beneficial for general thermal management in applications, such as uniform, porous heaters. TGA measurements in air (Figure 1d) indicate excellent thermal stability of the rGO aerogels at moderate temperatures. A small broad weight loss of about 2 wt%, observed between 100 and 400 °C, is likely to be associated with the evaporation of adsorbed moisture from the environment. Nanocarbon combustion does not occur below 400 °C (T_{onset} = 425 °C) which makes the rGO aerogels ideal candidates for support frameworks for catalyst and solid adsorber systems that require activation or regeneration in the medium temperature range up to 400 °C.
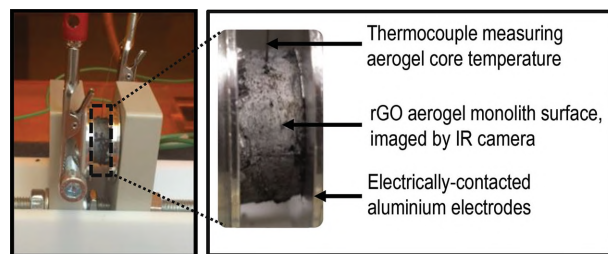
Figure 2. Setup for the measurement of the electrical and Joule-heating characteristics of nanocarbon aerogels.

2.2. Joule Heating Characteristics

In order to demonstrate direct Joule heating of the rGO aerogel, monoliths were inserted between two circular electrodes of a custom-made contacting rig (**Figure 2**) and compressed by about 10% of the original height to ensure a reliable and uniform, electrical contact area.

Electrical current and power applied to the aerogel was controlled and monitored by a potentiostat. Due to the thermal working limitations of the contacting rig material (PEEK), Joule heating was restricted to a maximum temperature of 200 °C. Aerogel Joule heating at steady-state conditions was visualized via IR imaging of the aerogel surface (**Figure 3**).

The thermal images (Figure 3a) indicate distinct control of the aerogel surface temperature between room temperature and 120 °C at low input voltages between 0.5 and 1.25 V. It is noteworthy that film heaters of comparable, two-dimensional size require an order of magnitude higher voltages to reach similar temperatures.[10b,10e,g] Figure 3b shows the surface temperature profiles in the axial direction of the cylindrical monolith (along the direction of the current flow) and transverse to the monolith axis. In the transverse direction, the aerogel surface temperature is uniform, with a sharp drop at the aerogel/air interface. Occasional small hot spots indicate structural imperfections in the aerogel which are likely to give rise to locally higher electrical fields, and therefore, slightly higher temperatures; however, the noise level in the transverse temperature profile is generally low. In contrast, a significant temperature gradient is observed in the axial temperature profile. This gradient is caused by the use of large-area, bulky metal electrodes in this study that act as effective heat sinks, leading to significantly decreased temperature in close proximity to the electrodes. Similar observations have been made for the surface temperature of film heaters contacted through evaporated gold electrodes.[10e] For the aerogels, this effect could, however, be minimized by the use of larger aerogel monoliths where the majority of the aerogel material is not adjacent to the electrodes or through the use of smaller, perforated electrodes minimizing heat sink effects.

The internal aerogel temperature at steady state conditions was measured by a thin thermocouple inserted into the monolith core centrally (furthest from the two electrodes). At the same voltage, the measured internal temperatures were considerably higher than the surface temperature, as expected for an uninsulated sample due to constant heat loss at the aerogel/air interface. The difference between the monolith
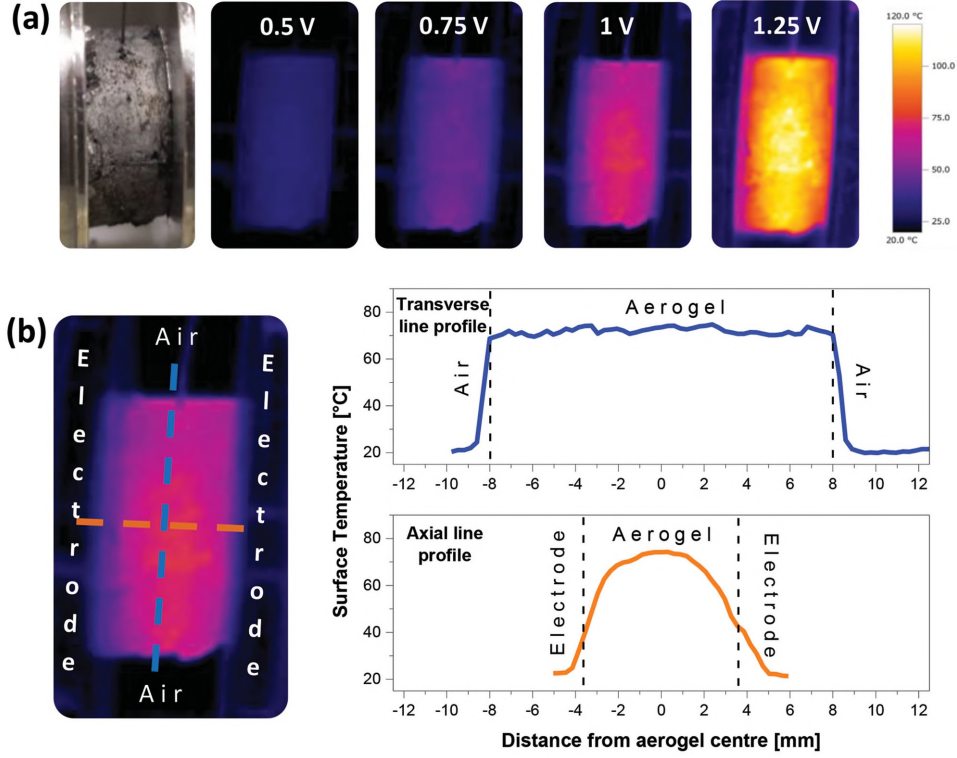
Figure 3. Surface temperature of rGO aerogel at steady state conditions: a) Thermal IR images of aerogel at different voltage inputs, b) temperature line profiles of Joule heated rGO aerogel (input voltage 1 V), measured transverse to the monolith axis (blue line) and in the axial direction of the monolith cylinder (orange line); dotted lines indicate the aerogel/air and aerogel/electrode interface, respectively.

core and surface temperature is dependent on the input power (**Figure 4**), that is, on the heat generated within the aerogel, and is a reflection of the thermal transport properties of the aerogel.
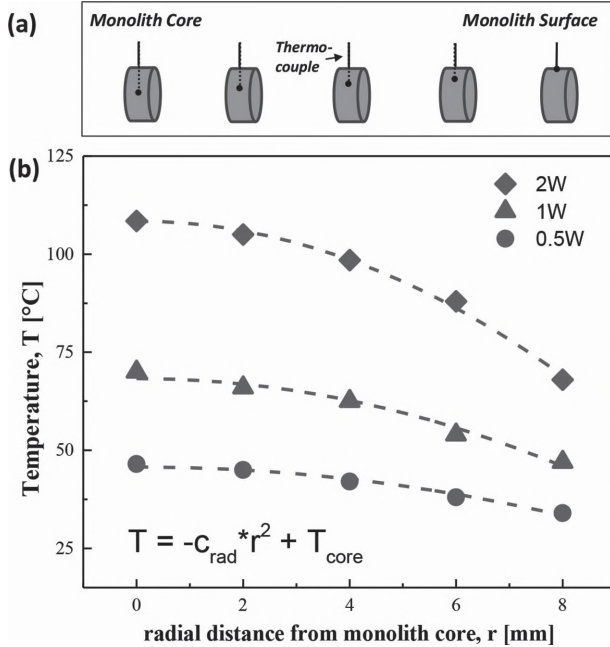
Figure 4. Radial temperature gradient of uninsulated rGO aerogel, Joule-heated at different inputs of electrical power.

The radial temperature gradients across the center of the uninsulated monolith are well fitted by a quadratic function (Figure 4) and can be analyzed by a highly simplified model of one-dimensional heat conduction in cylinders with homogeneous, internal energy generation:[19]

$$T = -\frac{qr^2}{4k} + T_{core} \tag{1}$$

where q is the energy density generated (here taken as input electrical power per unit volume), r is the distance from the monolith core, T_{core} a general integration constant (here the temperature at the aerogel core) and k the thermal conductivity of the aerogel.

Table 2 displays the power densities, the relevant quadratic fit parameters (c_{rad}, T_{core}), and the calculated thermal conductivities for the three different electrical power inputs (P).

Table 2. Thermal conductivities estimated from the radial temperature gradient of the rGO aerogels.

| P [W]	q [10^5 W m^{-3}]	T_{core} [°C]	c_{rad} [10^5 K m^{-3}]	k [W m^{-1} K^{-1}]
0.5	2.94	46	1.9	0.39
1	5.88	68	3.5	0.42
2	11.8	108	5.9	0.5

This approach provides an interesting, alternative method for the estimation of the thermal conductivity of nanocarbon aerogels as it does not require the input of other thermal material parameters, such as thermal diffusivity (δ) and specific heat capacity (c_p), which are often difficult to measure due to the low density, high porosity and small weight of aerogel samples. While being on the same order of magnitude, the k values determined through the analysis of the radial heat distribution (Table 2) are significantly higher compared to the ones measured through the more conventional flash methodology (Table 1 and Supporting Information, Figure S1). Systematic errors in both methodologies are likely to contribute to this discrepancy. Significant uncertainties in the flash method arise from the difficult experimental determination of c_p for ultralight nanocarbon aerogels while the simplified analysis of the radial temperature gradient does not account for axial heat losses into the electrodes (see Figure 3), likely resulting in an overestimation of q, and consequently k, in Equation 1. The latter effect could, however, be significantly minimized when using less bulky electrodes or larger samples, as discussed above. Further, laser flash measurements of k at different temperatures (Supporting Information, Figure S1) suggest that the thermal conductivity of the rGO aerogel increases with temperature in the range probed in this paper, contributing to the large k values in Table 2 and their increasing trend with electrical power input, that is, Joule-heating temperature. While the radial temperature gradient can be useful to analyze the thermal properties of nanocarbon aerogels, it is undesirable for practical applications as local heaters. However, simple engineering solutions using insulation and alternative geometries are widely known and could adjust the radial temperature homogeneity to the level required for a given application (Supporting Information, Figure S3).

The steady-state core temperatures were further analyzed in terms of temperature-voltage and temperature-power characteristics. The internal temperature increases with electrical voltage and power, reaching temperatures of around 180 °C at relatively low potential and electrical power input of 1.25 V and 3.7 W, respectively (**Figure 5**). The quadratic correlation of input voltage and temperature (Figure 5a) and the linear relationship of electrical power input and temperature (Figure 5b) are in agreement with Joule's law, indicating a complete conversion of electrical input power into heat and constant specific heat capacity over the temperature range probed.

In addition, the linear dependency between temperature increase and power input suggests that heat conduction into the electrodes and convective heat dissipation at the aerogel/air interface are the dominant heat loss pathways, as discussed above, while radiative energy losses (which would be indicated by a non-linear T^{-4} temperature-power relationship) do not play a significant role in the temperature range studied here. This finding is in good agreement with the characteristics of two-dimensional film heaters[10d] where significant radiative emission losses only occur above 200 °C. However, in contrast to many nanocarbon film heaters, the rGO aerogel electrical resistance and conductivity are virtually temperature-independent up to 200 °C (Figure 5a, inset). In this temperature range, thin nanocarbon films have shown significantly increased
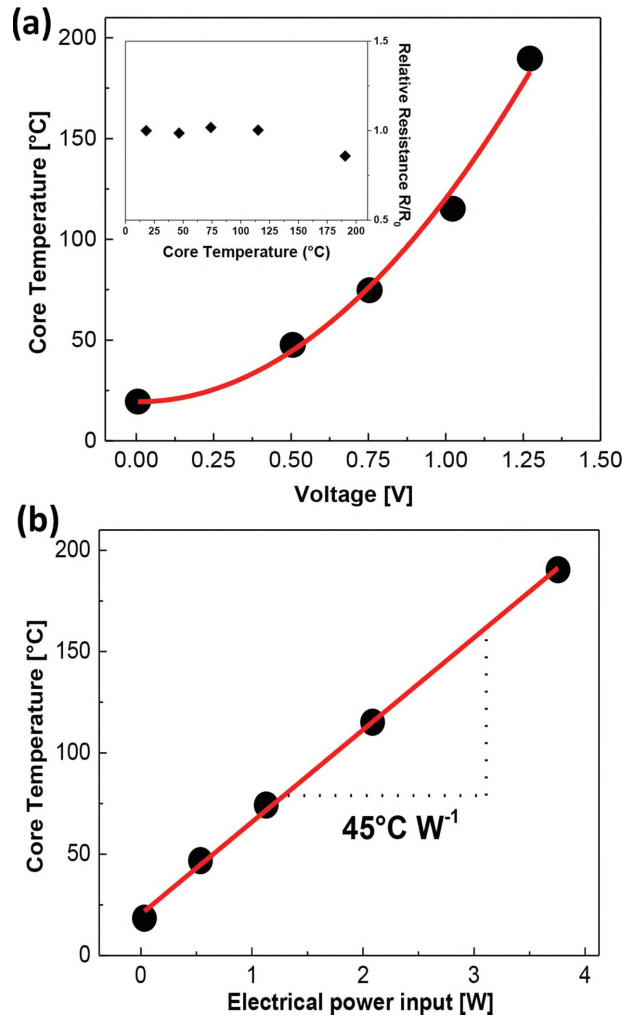
Figure 5. Core temperature of rGO aerogel at steady-state conditions: a) core temperature as function of input voltage; inset: relative resistance, R/R_0, at different temperatures; b) core temperature as function of electrical power input.

resistances, up to 20% of their room temperature values.[10e] However, investigations on free-standing carbon nanotube films have shown that preconditioning through voltage cycling, as applied in this study, can reduce this temperature sensitivity dramatically.[10d]

The heating performance of film heaters has been described in terms of temperature increase per electrical input power, dT/dP.[10e] The rGO aerogel exhibits a dT/dP value of 45 °C W^{-1} (or dT/dq = 76 °C cm^3 W^{-1} in terms of power density). In absolute terms, this value is on the same order of magnitude as dT/dP values of nanocarbon films with comparable dimensions (30–150 °C W^{-1}),[10c–f,20] suggesting comparable heating efficiencies of 2D and 3D assemblies. A more detailed comparison between nanocarbon films and aerogels in terms of heating performance per sample volume or mass is not possible due to limited information in the film heater literature. Nevertheless, the dT/dP gradient of the Joule heated rGO aerogel indicates that, at the same electrical power input, the rGO aerogel reaches similar temperatures as comparable nanocarbon films.

Joule heating at 1 W   Cooling by natural convection
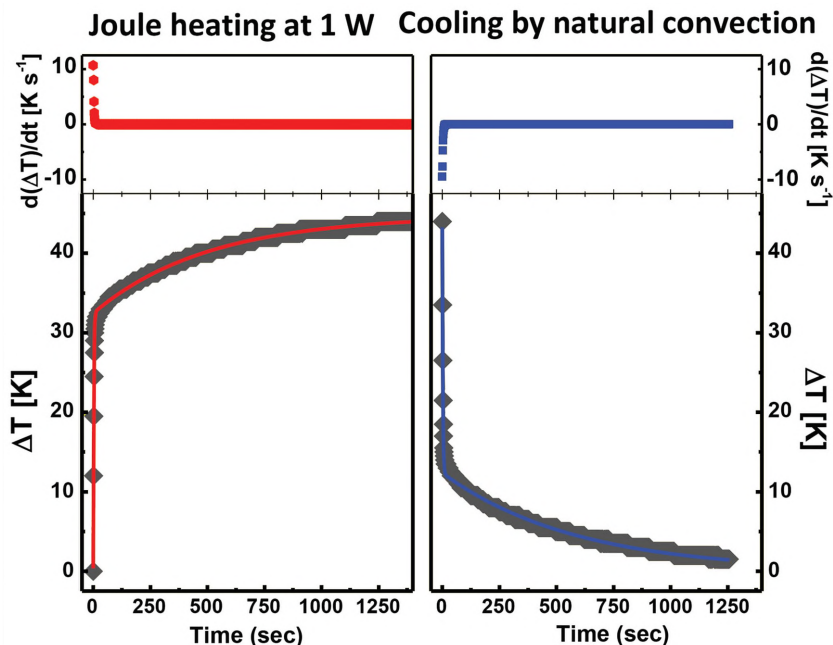
Figure 6. Evolution of the temperature change, ΔT, (i.e., difference between the core temperature of an uninsulated rGO aerogel and the environment temperature) with time at 0.75 V.

The temperature profile clearly indicates two distinct heating phases. In the initial heating regime the temperature increases very rapidly with an initial heating rate of up to 10 K s^{-1}, comparable to the fast Joule heating rates of (substrate-supported) nanocarbon film heaters and carbon fibers, reported in the literature.[10e,10g] In this short initial phase (around 2 s, see also Supporting Information, Table S3), heat losses to the environment and the electrodes are minimal and the heating is approximately adiabatic. This fast heating is followed by a considerably slower heating regime (heating rates around 0.01 K s^{-1}), likely to be dominated by conductive and convective heat losses. The second heating phase is orders of magnitude longer than observed in nanocarbon films, probably due to lengthy temperature equilibration between the environment and the porous interior of the aerogel. This two-regime behavior is mirrored for the cooling of the uninsulated aerogel by natural convection, where a first rapid cooling phase (cooling rates up to –10 K s^{-1}) is followed by a second, slower equilibration phase. The Joule heating behavior in the fast heating/cooling regime was further investigated via voltage cycling measurements performed at comparatively fast rates of 25 mV s^{-1} and short step times (1 s/step), applying peak voltages that gave rise to temperature increases of more than 10 °C (**Figure 7**).

However, its significantly lower electrical conductivity enables Joule-heating of the rGO aerogel at an order of magnitude lower applied voltages compared to typical nanocarbon films.

Further information on the Joule heating characteristics can be gained when measuring the temperature evolution of the aerogel at constant power input. **Figure 6** shows a typical Joule heating response of the uninsulated rGO aerogel.

Under these cyclic conditions, the temperature increases linearly with the electrical power input, similar to the observations
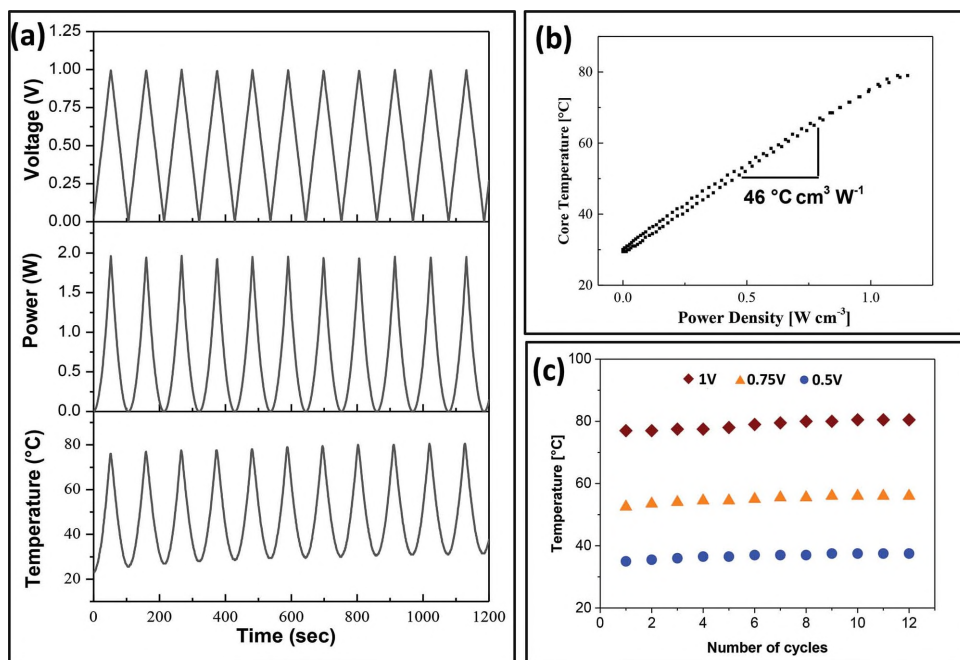
Figure 7. Joule heating cycling: a) Voltage cycling between 0 and 1 V at 25 mV s^{-1} and Joule heating response; b) Power-temperature relationship of the fifth cycle; c) Peak temperatures for 12 cycles at different maximum voltages.

made at steady-state conditions, however at a shallower gradient due to the limited energy input into the aerogel at fast cycling rates and short step times. Importantly, the aerogel temperature also decreases linearly at a similar gradient when cycling voltage, and therefore power input, is decreased. The resulting lack of hysteresis between heating and cooling branch of each cycle enables repeated and reproducible temperature cycling, reaching distinct peak temperatures at set voltages (Figure 7c). These fast cycling characteristics highlight the advantages of using a nanocarbon aerogels for applications that require extensive, fast temperature cycling.

3. Conclusion

Direct resistive heating of light-weight, compressible, porous rGO aerogel monoliths has been demonstrated. The rGO aerogels investigated showed high electrical conductivity, large accessible porosity and high thermal conductivity. At steady-state conditions, the voltage-temperature characteristics indicate efficient heating at comparatively low voltages, reaching temperatures of about 200 °C at about 1.3 V and power densities of about 2.5 W cm^{-3}. Since power generation per unit volume is constant, adjustable uniform temperature is in principle available in large aerogel monoliths, offering convenient, low-voltage heating in a scalable way. The linear correlation of electrical power density and temperature (dT/dq = 76 °C cm^3 W^{-1}) suggests conductive and convective heat losses as main heat dissipation pathways in the studied temperature regime and a heating performance comparable to two-dimensional nanocarbon film heaters. When thermally uninsulated, the rGO aerogels show characteristic, fast heating and cooling rates of up to 10 K s^{-1} during the initial kinetic time regime. Analysis of the radial temperature gradient of the aerogels can be used for straightforward estimation of the thermal conductivity without need for other thermal material parameters. Within the fast heating/cooling regime, reproducible temperature cycling has been demonstrated. These characteristics should enable quick and uniform temperature control of the permeating gas within the porous nanocarbon network or of functional particles supported on the graphitic framework. The combination of these excellent Joule heating characteristics with other, well-established benefits (e.g., light weight, high-surface area, chemical inertness etc.) makes nanocarbon aerogels highly interesting candidates for energy-efficient and homogeneous flow-through heating systems in catalysis and solid adsorbent regeneration.

4. Experimental Section

Fabrication of Nanocarbon Aerogels: Graphene oxide (GO) solutions were prepared using the modified Hummers method[21] and subsequently centrifuged at 9000 rpm for 2 h in order to obtain concentrated GO solutions. The rGO aerogels were produced following a previously developed emulsion-templating methodology.[13] Organic additives (PVA:sucrose in a 1:1 fixed ratio) were added to the concentrated GO solutions, using an ultrasonic tip (UP200S, Hielscher) to obtain homogeneous 1.6 wt% nanocarbon suspensions. The aqueous nanocarbon suspensions were emulsified with a hydrophobic phase

(toluene) in a 1:1 fixed volume ratio by hand shaking. The nanocarbon emulsion was cast into cylindrical Teflon moulds and unidirectionally frozen at 10 K min^{-1} in a house built freeze caster. Bulk nanocarbon monoliths with cylindrical shape of ≈16 mm in diameter and 8 mm in height were obtained by freeze-drying (Freezone 4.5, Labconco Corporation). The nanocarbon monoliths were then thermally reduced at 1000 °C in 10%H$_2$/90%Ar atmosphere inside a tubular oven (Carbolite Furnaces) to produce the final reduced GO (rGO) monoliths. While the resulting materials can be properly described as cryogels with cellular network structure, the produced bulk materials are referred to as aerogels in this paper for simplicity, following similar nomenclature in the literature using the term "aerogel" for ultralight, gas-filled nanocarbon 3D assemblies in general, regardless of processing details.[4,15]

General Characterization of Nanocarbon Aerogels: The aerogel envelop density, ρ_{env}, was estimated as the ratio of monolith weight over monolith volume. The skeletal aerogel density, ρ_{sk}, was determined via the gas displacement method in an AccuPyc 1330 (Micromeritics, GA, U.S.A.), using helium (BOC, Essex, UK) with fill pressure 19.5 psig. Thermogravimetric analysis (TGA) was carried out using a Perkin-Elmer Pyris 1 TGA instrument. Experiments were performed in a temperature range between 50 and 850 °C under air flow (flow rate 10 mL min^{-1}), applying a constant ramp rate of 10 K min^{-1}. The combustion onset point (T_{onset}) was determined as the temperature at which the sample had lost 2 wt% of its initial weight.[22] Scanning electron microscopy (SEM) images were obtained on a GEMINI LEO 1525 FEGSEM instrument at an accelerating voltage of 5 kV; fragments of the rGO aerogel were fixed to a SEM stub by a carbon adhesive disk. The thermal conductivity (k, W m^{-1} K^{-1}) in Table 1 was calculated from the thermal diffusivity (δ, m^2 s^{-1}), the specific heat capacity (c_p, J g^{-1} K^{-1}) and the envelop density (ρ_{env}, g m^{-3}) according to:

$$k = \delta c_p \rho_{env} \tag{2}$$

Thermal diffusivity was measured by the laser flash method (NETZSCH Instruments Co., LFA 427 system), using a heating rate of 10 °C min^{-1}, and applying the "Cowan+pulse correction" diffusivity model for the processing of the data. The specific heat capacity, c_p, was measured on the same equipment using a reference sample of pure graphite.

Electrical and Joule Heating Characterization: All experiments were carried out in air within a sealable, custom-built Perspex box with gas inlets and electrical cable feed-throughs. Samples were studied within a custom-made, electrically contactable sample holder (Figure 2) consisting of two, large circular aluminium electrodes within two movable, heat-resistant PEEK holder blocks that enabled controlled sample compression of the elastic aerogel monoliths. Preliminary experiments showed that ensuring good thermal and electrical contact between the electrode and the aerogel is crucial to obtain reliable and repeatable Joule heating results. Following other literature reports on nanocarbon aerogels,[4,17] silver paste was used to reduce contact resistance, and did not permeate the samples. Further, measurements were carried out at an aerogel compression strain of 10%, unless otherwise stated. The electrical current was controlled using a potentiostat (1281 Multiplexer, Solatron Analytical). Samples were preconditioned before any measurement through repeated voltage cycling between 0 and 1.5 V to drive off any residual moisture. The electrical conductivity is determined from the electrical aerogel resistance (R, Ω), as well as the aerogel contact area (A, 2.3 cm^2) and the monolith length (L, 0.73 cm). The electrical resistance is taken as the gradient of the linear I–V curve (see Figure 1). Joule heating of the aerogel surface was visualised using a thermal IR camera (Testo 880–1, Testo Inc), temperature profiles were analysed using the associated Testo IRSoft software. The internal aerogel temperature was measured using a thin (0.25 mm diameter) K-type thermocouple (TJC 120 Series, sheath stainless steel, ungrounded, Omega UK) inserted into the monolith core, using a data logger (EL-USB-TC, Lascar Electronics) for continuous temperature read out. Steady-state conditions were assumed to have been reached after 30 min.

Supporting Information

Acknowledgements

[1] a) A. Javey, J. Guo, Q. Wang, M. Lundstrom, H. Dai, *Nature* **2003**, *424*, 654; b) M. Orlita, C. Faugeras, P. Plochocka, P. Neugebauer, G. Martinez, D. K. Maude, A. L. Barra, M. Sprinkle, C. Berger, W. A. de Heer, M. Potemski, *Phys. Rev. Lett.* **2008**, *101*, 267601.

[2] a) E. Pop, D. Mann, Q. Wang, K. Goodson, H. Dai, *Nano Lett.* **2005**, *6*, 96; b) A. A. Balandin, S. Ghosh, W. Bao, I. Calizo, D. Teweldebrhan, F. Miao, C. N. Lau, *Nano Lett.* **2008**, *8*, 902.

[3] a) C. Lee, X. Wei, J. W. Kysar, J. Hone, *Science* **2008**, *321*, 385; b) M.-F. Yu, B. S. Files, S. Arepalli, R. S. Ruoff, *Phys. Rev. Lett.* **2000**, *84*, 5552.

[4] a) S. Nardecchia, D. Carriazo, M. L. Ferrer, M. C. Gutierrez, F. del Monte, *Chem. Soc. Rev.* **2013**, *42*, 794; b) M. B. Bryning, D. E. Milkie, M. F. Islam, L. A. Hough, J. M. Kikkawa, A. G. Yodh, *Adv. Mater.* **2007**, *19*, 661; c) F. Liu, T. S. Seo, *Adv. Funct. Mater.* **2010**, *20*, 1930; d) M. C. Gutiérrez, M. J. Hortigüela, J. M. Amarilla, R. Jiménez, M. L. Ferrer, F. del Monte, *J. Phys. Chem. C* **2007**, *111*, 5557; e) J. Zou, J. Liu, A. S. Karakoti, A. Kumar, D. Joung, Q. Li, S. I. Khondaker, S. Seal, L. Zhai, *ACS Nano* **2010**, *4*, 7293; f) M. A. Worsley, S. O. Kucheyev, J. H. Satcher, A. V. Hamza, T. F. Baumann, *Appl. Phys. Lett.* **2009**, *94*; g) M. A. Worsley, T. Y. Olson, J. R. I. Lee, T. M. Willey, M. H. Nielsen, S. K. Roberts, P. J. Pauzauskie, J. Biener, J. H. Satcher, T. F. Baumann, *J. Phys. Chem. Lett.* **2011**, *2*, 921; h) Z. Tang, S. Shen, J. Zhuang, X. Wang, *Angew. Chem., Int. Ed.* **2010**, *49*, 4603; i) H. Bai, C. Li, X. Wang, G. Shi, *Chem. Comm.* **2010**, *46*, 2376; j) H. Bai, C. Li, X. Wang, G. Shi, *J. Phys. Chem. C* **2011**, *115*, 5545; k) Y. Xu, Q. Wu, Y. Sun, H. Bai, G. Shi, *ACS Nano* **2010**, *4*, 7358; l) H. Huang, P. Chen, X. Zhang, Y. Lu, W. Zhan, *Small* **2013**, *9*, 1397.

[5] a) R. K. Das, B. Liu, J. R. Reynolds, A. G. Rinzler, *Nano Lett.* **2009**, *9*, 677; b) B. G. Choi, M. Yang, W. H. Hong, J. W. Choi, Y. S. Huh, *ACS Nano* **2012**, *6*, 4020; c) Y. Sun, Q. Wu, G. Shi, *Phys. Chem. Chem. Phys.* **2011**, *13*, 17249; d) M. C. Gutiérrez, D. Carriazo, A. Tamayo, R. Jiménez, F. Picó, J. M. Rojo, M. L. Ferrer, F. del Monte, *Chem. Eur. J.* **2011**, *17*, 10533.

[6] a) F. Yavari, Z. Chen, A. V. Thomas, W. Ren, H.-M. Cheng, N. Koratkar, *Sci. Rep.* **2011**, *1*; b) X. Dong, Y. Ma, G. Zhu, Y. Huang, J. Wang, M. B. Chan-Park, L. Wang, W. Huang, P. Chen, *J. Mater. Chem.* **2012**, *22*, 17044.

[7] a) S. Lu, Y. Liu, *Appl. Catal., B* **2012**, *111–112*, 492; b) H. Li, X. Gui, C. Ji, P. Li, Z. Li, L. Zhang, E. Shi, K. Zhu, J. Wei, K. Wang, H. Zhu, D. Wu, A. Cao, *Nano Res.* **2012**, *5*, 265; c) Y. Long, C. Zhang, X. Wang, J. Gao, W. Wang, Y. Liu, *J. Mater. Chem.* **2011**, *21*, 13934; d) T. Sun, Z. Zhang, J. Xiao, C. Chen, F. Xiao, S. Wang, Y. Liu, *Sci. Rep.* **2013**, *3*; e) L. Chen, B. Wei, X. Zhang, C. Li, *Small* **2013**, *9*, 2331.

[8] a) X. Gui, J. Wei, K. Wang, A. Cao, H. Zhu, Y. Jia, Q. Shu, D. Wu, *Adv. Mater.* **2010**, *22*, 617; b) K. C. Kemp, H. Seema, M. Saleh, N. H. Le, K. Mahesh, V. Chandra, K. S. Kim, *Nanoscale* **2013**, *5*, 3149; c) F. Ding, Y. Lin, P. O. Krasnov, B. I. Yakobson, *J. Chem. Phys.* **2007**, *127*; d) H.-P. Cong, X.-C. Ren, P. Wang, S.-H. Yu, *ACS Nano* **2012**, *6*, 2693; e) Z. Sui, Q. Meng, X. Zhang, R. Ma, B. Cao, *J. Mater. Chem.* **2012**, *22*, 8767.

[9] a) H. Maune, H.-Y. Chiu, M. Bockrath, *Appl. Phys. Lett.* **2006**, *89*; b) H. Y. Chiu, V. V. Deshpande, H. W. C. Postma, C. N. Lau, C. Mikó, L. Forró, M. Bockrath, *Phys. Rev. Lett.* **2005**, *95*, 226101; c) E. Pop, *Nanotechnol.* **2008**, 19.

[10] a) Z. P. Wu, J. N. Wang, *Physica E* **2009**, *42*, 77; b) D. Sui, Y. Huang, L. Huang, J. Liang, Y. Ma, Y. Chen, *Small* **2011**, *7*, 3186; c) H.-S. Jang, S. K. Jeon, S. H. Nahm, *Carbon* **2011**, *49*, 111; d) D. Janas, K. K. Koziol, *Carbon* **2013**, *59*, 457; e) T. J. Kang, T. Kim, S. M. Seo, Y. J. Park, Y. H. Kim, *Carbon* **2011**, *49*, 1087; f) J. J. Bae, S. C. Lim, G. H. Han, Y. W. Jo, D. L. Doung, E. S. Kim, S. J. Chae, T. Q. Huy, N. Van Luan, Y. H. Lee, *Adv. Funct. Mater.* **2012**, *22*, 4819; g) D. Janas, K. K. Koziol, *Nanoscale* **2014**, *6*, 3037.

[11] B. Mas, J. P. Fernández-Blázquez, J. Duval, H. Bunyan, J. J. Vilatela, *Carbon* **2013**, *63*, 523.

[12] V. Roberto Guzmán de, Y. Namiko, M. Antonio, L. W. Brian, *Nanotechnology* **2011**, *22*, 185502.

[13] S. Barg, F. M. Perez, P. V. Pereira, N. Na, R. Maher, E. Garcia-Tunon, S. Eslava, S. Agnoli, C. Mattevi, E. Saiz, *Nat. Commun.* **2014**, *5*, 4328.

[14] M. Diba, A. García-Gallastegui, R. N. Klupp Taylor, F. Pishbin, M. P. Ryan, M. S. P. Shaffer, A. R. Boccaccini, *Carbon* **2014**, *67*, 656.

[15] H. Sun, Z. Xu, C. Gao, *Adv. Mater.* **2013**, *25*, 2554.

[16] Z. Fan, D. Z. Y. Tng, S. T. Nguyen, J. Feng, C. Lin, P. Xiao, L. Lu, H. M. Duong, *Chem. Phys. Lett.* **2013**, *561–562*, 92.

[17] a) K. H. Kim, Y. Oh, M. F. Islam, *Adv. Funct. Mater.* **2013**, *23*, 377; b) M. A. Worsley, P. J. Pauzauskie, T. Y. Olson, J. Biener, J. H. Satcher, T. F. Baumann, *J. Am. Chem. Soc.* **2010**, *132*, 14067.

[18] a) S. N. Schiffres, K. H. Kim, L. Hu, A. J. H. McGaughey, M. F. Islam, J. A. Malen, *Adv. Funct. Mater.* **2012**, *22*, 5251; b) K. J. Zhang, A. Yadav, K. H. Kim, Y. Oh, M. F. Islam, C. Uher, K. P. Pipe, *Adv. Mater.* **2013**, *25*, 2926.

[19] J. R. Welty, C. E. Wicks, R. E. Wilson, G. Rorrer, *Fundamentals of Momentum, Heat, and Mass Transfer*, Wiley, Hoboken, NJ, USA **2001**.

[20] P. Liu, L. Liu, K. Jiang, S. Fan, *Small* **2011**, *7*, 732.

[21] W. S. Hummers, R. E. Offeman, *J. Am. Chem. Soc.* **1958**, *80*, 1339.

[22] R. Menzel, A. Lee, A. Bismarck, M. S. P. Shaffer, *Langmuir* **2009**, *25*, 8340.